Powertrain sizing of electrically supercharged internal combustion engine vehicles

Nikolce Murgovski [*] **Sava Marinkov** [**] **Daniël Hilgersom** [**]
Bram de Jager [**] **Maarten Steinbuch** [**] **Jonas Sjöberg** [*]

[*] *Department of Signals and Systems, Chalmers University of Technology, 41296 Gothenburg, Sweden (e-mail: nikolce.murgovski@chalmers.se).*
[**] *Department of Mechanical Engineering, Eindhoven University of Technology, P.O. Box 513, 5600 MB Eindhoven, The Netherlands.*

Abstract: We assess the concept of electrically supercharged internal combustion engines, where the supercharger, consisting of a compressor and an electric motor, draws electric power from a buffer (a battery or a supercapacitor). In particular, we investigate the scenario of downsizing the engine, while delivering high power demands by supercharging. Simultaneously, we seek the optimum buffer size that provides sufficient electric power and energy to run the supercharger, such that the vehicle is able to deliver the performance required by a driving cycle representing the typical daily usage of the vehicle. We provide convex modeling steps that formulate the problem as a second order cone program that not only delivers the optimal engine and buffer size, but also provides the optimal control and state trajectories for a given gear selection strategy. Finally, we provide a case study of sizing the engine and the electric buffer for different compressor power ratings.

Keywords: electric supercharger, convex optimization, powertrain design, energy management, optimal control

1. INTRODUCTION

Recent years have shown high interest in the reduction of energy consumption and pollutant emissions of ground transportation. With the goal of improving energy efficiency and employing renewable energy sources, vehicle manufactures are currently introducing several types of electrified vehicles. Nevertheless, the internal combustion engines (ICE) are expected to remain the dominant force in the automotive market for decades to come [Shahed and Bauer, 2009].

To meet the ever-tightening expectations on fuel economy, the automotive industry has pursued the path of engine downsizing [Leduc et al., 2003]. The latter is often followed by a practice of ICE overpowering to improve the vehicle drivability. In general this also results in reduced carbon emissions and a better fuel economy compared to a larger engine, mainly due to the reductions in engine weight, friction and throttle valve losses [Fraser et al., 2009]. ICE overpowering is made possible by the use of boosting devices such as a turbocharger (driven by hot exhaust gases) or a supercharger (driven mechanically by the crank shaft via a chain or belt). In both cases, a compressor increases (boosts) the pressure or density of the air supplied to the engine, providing the engine with more oxygen (air). This allows more fuel to be injected and burned, thereby increasing the ICE maximum torque and power limits.

However, turbo-charged ICEs exhibit a relatively low-torque capability at low engine speeds [Taylor and Howe, 2007] which compromises vehicle drivability and acceleration performance. Namely, at low speed the downsized ICEs suffer from the insufficient exhaust gas-flow to adequately propel the turbocharger at the moment the gas pedal is pressed, inducing the well-known turbo-lag [Leduc et al., 2003]. The belt-driven supercharger, on the other hand, does not experience the turbo-lag phenomenon, but is less fuel economic as it increases the engine parasitic losses. One way to efficiently provide the required low-end torque and at the same time eliminate the turbo-surge/lag is to electrify the mechanical superchargers, *i.e.,* replace/equip their mechanical power source (prime mover) with an electric motor [Villegas et al., 2011, Chayopitak et al., 2012, Kachapornkul et al., 2012, Wang et al., 2005]. The resulting device, an electric supercharger, *i.e.,* a motor-compressor unit (MCU), follows a popular automotive trend of vehicle electrification that has already proven capable of improving the efficiency and performance of numerous systems such as the steering, water pump and air conditioning. The success achieved by electrification so far is primarily due to the electric machine's ability to efficiently produce the requested, instantaneous torque in a remarkably wide speed range, from zero to several hundred thousands rotations per minute.

Historically, the lack of compact, high-power/energy-density electric sources and of light-weight, high-speed, high-power-density electric motors prohibited the prolif-

eration of the MCU devices throughout the automotive sector. The widely used 12 V battery system is at the limit of providing sufficient power for the electrical boost [Taylor and Howe, 2007]. Besides, the high power surges from the MCU may incur high battery losses.

Today the situation regarding electric storage elements is somewhat different as a plethora of high-power batteries and high-energy capacitors appear on the market. However, the choice of electric buffer technology and the optimal buffer size in terms of power ratings and energy density is still an open question.

In this paper we seek the optimum buffer size that provides sufficient electric power and energy to run the supercharger, such that the vehicle is able to drive a representative driving cycle. Besides sizing the buffer, we also investigate the scenario of downsizing the ICE, while delivering high power demands by supercharging. The resulting optimization problem is a dynamic program, where the ICE and buffer are optimal sized only when the vehicle is also optimally controlled on the studied driving cycle. The problem is non-convex, nonlinear and mixed-integer dynamic program, where both plant design and control are optimization variables.

The plant design and control problem is typically handled by decoupling the plant and controller, and then optimizing them sequentially or iteratively [Assanis et al., 1999, Galdi et al., 2001, Wu et al., 2011, Fathy et al., 2004, Peters et al., 2013]. However, sequential and iterative strategies generally fail to achieve global optimality [Reyer and Papalambros, 2002]. An alternative is a nested optimization strategy, where an outer loop optimizes system's objective over the set of feasible plants, and an inner loop generates optimal controls for plants chosen by the outer loop [Fathy et al., 2004]. This approach delivers the globally optimal solution, but it may incur heavy computational burden (when, e.g., dynamic programming is used to optimize the energy management [Tara et al., 2010]), or may require substantial modeling approximations [Filipi et al., 2004, Kim and Peng, 2007, Sundström et al., 2010].

This paper addresses the problem by first decoupling the integer decisions, *i.e.,* the gear selection strategy, and then formulating the remaining problem as a convex second order cone program (SOCP) [Boyd and Vandenberghe, 2004]. The integer signals are decided outside the convex program, by using a simple heuristic strategy that has been observed to give near optimal results for the problem of sizing series and parallel hybrid electric vehicle powertrains [Murgovski et al., 2012c, Pourabdollah et al., 2013].

Finally, a case study is provided that depicts the optimal engine and electric buffer sizes for different compressor power ratings and two buffer technologies, a lithium-ion battery and a supercapacitor.

This paper is organized as follows. Section 2 provides background to the electrically supercharged ICE configuration and states a verbal problem formulation. The mathematical modeling is provided in Section 3 and the convex optimization problem is formulated in Section 4. Section 5 presents a use-case study. Discussion and conclusions are drawn in Section 6.

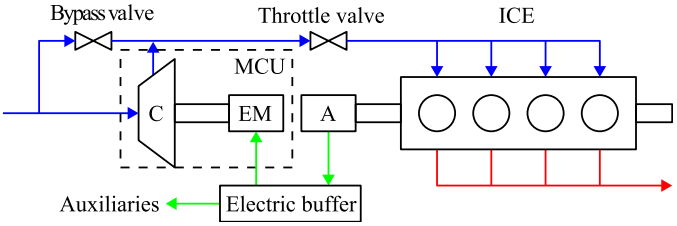

Fig. 1. ICE equipped with a stand-alone motor-compressor unit (MCU). The electric buffer is discharged by auxiliary loads and the electric motor (EM), which in turn drives the compressor (C). The buffer is charged by the conventional car-alternator (A), which is driven by the internal combustion engine (ICE).

Table 1. Optimization problem for powertrain components sizing and energy management.

Minimize:
Operational + component cost;
Subject to:
Driving cycle constraints,
Energy conversion and balance constraints,
Buffer dynamics,
Physical limits of components,
...
(For all time instances along the driving cycle).

2. THE POWERTRAIN SIZING PROBLEM

The block diagram of the ICE electrically supercharged with an MCU is illustrated in Fig. 1. The MCU, which is placed in the ICE air intake along with a bypass valve, enables more power to be delivered from the ICE, *e.g.,* while overtaking or when starting-off at traffic lights. When the excess power is needed, which we refer to as supercharging, the bypass valve is closed, while it is open during naturally-aspirated operation.

The bursts of mechanical MCU power have to be matched by the power ratings of the electric buffer that drives the MCU. However, deciding the optimal buffer energy requirement is not trivial, since this depends on the typical daily usage of the vehicle. A common form of representing the vehicle usage is by recording speed and acceleration profiles for a period of time, and then constructing a driving cycle that contains both the vehicle speed and road topography as functions of time. An example of such cycle is the Class 3 World Harmonized Light Vehicle Test Procedure [1] (WLTP3), which is used here as a proof of concept for realization of the method being proposed.

The vehicle is required to exactly follow the speed demanded by the driving cycle (in a backwards simulation approach), thus ensuring that a possible downsizing of the powertrain does not compromise the demanded performance. To have a fair comparison, the buffer is required to sustain its initial charge at the end of the driving cycle, meaning that any energy used for supercharging has to be put back in the buffer at some point, through the conventional car-alternator driven by the ICE. This may require high utilization of the electric buffer, making it beneficial to increase its size. However, a larger buffer increases the cost of the vehicle. Then, to keep the cost

[1] http://www.dieselnet.com/standards/cycles, March 2015.

down, the possibility of downsizing the ICE is also considered, such that the optimal tradeoff is reached between the components cost and the operational cost within the lifetime of the vehicle.

The resulting optimization problem is verbally stated in Table 1, while the mathematical description is deferred to Section 3.

3. MODELING AND PROBLEM FORMULATION

The optimization problem formulated in Table 1 is revisited here, by providing mathematical meaning to constraints and the objective function.

3.1 Longitudinal dynamics and power balance

The vehicle is modeled as a point mass system, where the vehicle mass

$$m(\cdot) = m_0 + m_{\mathrm{E}} s_{\mathrm{E}} + m_{\mathrm{B}} s_{\mathrm{B}} \tag{1}$$

consists of a baseline mass m_0 and a part varying linearly with scaling coefficients of the engine and buffer, s_E and s_B. The notation $(\cdot)$ is used to indicate a function of decision variables. The longitudinal relations of the point mass system can be described by the speed and torque demanded at the ICE shaft

$$\omega_d(t) = v(t)\frac{r_\gamma(t)}{r_w}, \tag{2}$$

$$\begin{aligned}\tau_d(\cdot) = {} & \frac{r_w^2 \lambda \dot{\omega}_d(t)}{r_\gamma^2(t)\eta_\gamma(t)} m(\cdot) + \frac{r_w g \sin\alpha(t)}{r_\gamma(t)\eta_\gamma(t)} m(\cdot) \\ & + \frac{\rho_a c_d A_f r_w^3 \omega_d^2(t)}{2 r_\gamma^3(t)\eta_\gamma(t)} + \frac{r_w g c_r \cos\alpha(t)}{r_\gamma(t)\eta_\gamma(t)} m(\cdot),\end{aligned} \tag{3}$$

where the last two terms in (3) are dissipative torques due to aerodynamic drag and rolling resistance. Here, r_w is wheels radius, λ is rotational mass ratio, ρ_a is air density, c_d is drag coefficient, A_f is vehicle's frontal area, c_r is rolling resistance coefficient, g is gravity, $\alpha(t)$ and $v(t)$ are speed and road slope provided by the driving cycle and r_γ and η_γ are ratio and efficiency of transmission gear $\gamma(t)$, including the final differential gear. Using (1) in (3) allows the demanded torque to be written as affine function of the scaling coefficients

$$\tau_d(\cdot) = \tau_0(t) + \tau_1(t) s_{\mathrm{E}} + \tau_2(t) s_{\mathrm{B}} \tag{4}$$

where for a given gear trajectory $\gamma(t)$, the torque trajectories $\tau_0(t), \tau_1(t), \tau_2(t)$ are defined at each time instant along the driving cycle.

The demanded torque is delivered by the ICE

$$\tau_{\mathrm{E}}(t) + \tau_{\mathrm{brk}}(t) = \frac{P_{\mathrm{A}}(t)}{\omega_{\mathrm{E}}(t)\eta_{\mathrm{A}}} + \tau_d(\cdot) \tag{5}$$

where $\tau_{\mathrm{E}}(t), \omega_{\mathrm{E}}(t)$ are engine torque and speed, $P_{\mathrm{A}}(t)$ and η_{A} are electric power and efficiency of the alternator and $\tau_{\mathrm{brk}}(t)$ is braking torque that includes the torque dissipated due to engine friction or usage of the braking pads. The relation between the ICE speed and the demanded speed is given by

$$\omega_{\mathrm{E}}(t) = \max\{\omega_d(t), \omega_{\mathrm{Eidle}}\} \tag{6}$$

where ω_{Eidle} is the engine idling speed.

The electric power balance is described by

$$P_{\mathrm{B}}(t) + P_{\mathrm{A}}(t) = P_{\mathrm{Bd}}(\cdot) + \frac{P_{\mathrm{C}}(\cdot)}{\eta_{\mathrm{M}}} + P_{\mathrm{aux}} \tag{7}$$

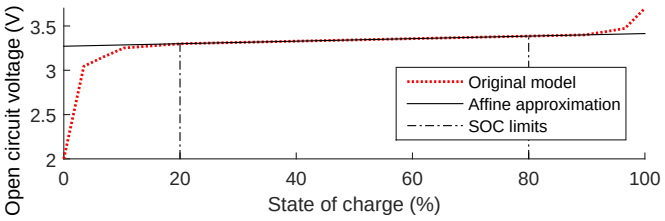

Fig. 2. Battery cell open circuit voltage.

where $P_{\mathrm{C}}(t)$ is mechanical MCU power, η_{M} is efficiency of the electric motor and power electronics running the compressor, P_{aux} is power consumed by auxiliary devices and $P_{\mathrm{B}}(t)$ and $P_{\mathrm{Bd}}(\cdot)$ are internal (before losses) and dissipative buffer powers. Positive value for $P_{\mathrm{B}}(t)$ in this context refers to discharging the buffer.

3.2 Electric buffer

The electric buffer pack is built of baseline number of n_0 cells connected in series, where the cells are either lithium-ion batteries, or supercapacitors. The battery cell is modeled as an open circuit voltage $u_c(\mathrm{soc})$ and a constant resistance R_c connected in series. The open circuit voltage is approximated as affine in state of charge (SOC)

$$u_c(\mathrm{soc}) = \frac{Q_c}{C_c}\mathrm{soc}(t) + u_{c0}, \tag{8}$$

where Q_c is cell capacity in Ah, while C_c (F) and u_{c0} (V) are coefficients obtained by fitting an affine relation to the cell open circuit voltage model, as illustrated in Fig. 2. Such approximation is suitable for lithium-ion battery technology, where operation at too low and high state of charge is avoided due to battery longevity reasons [Guzzella and Sciarretta, 2013].

When scaling the electric buffer, it is assumed that the baseline number of cells is multiplied by the scaling coefficient s_{B}. In the following, we employ the convex modeling steps of Murgovski et al. [2012b], where instead of cell voltage and cell current $i_c(t)$, decision variables are pack energy and power.

The pack energy is computed as

$$\begin{aligned}E_{\mathrm{B}}(t) &= s_{\mathrm{B}} n_0 Q_c \int_0^{\mathrm{soc}(t)} u_c(s)ds \\ &= \frac{s_{\mathrm{B}} n_0 C_c}{2}(u_c^2(\mathrm{soc}) - u_{c0}^2).\end{aligned} \tag{9}$$

Then, the pack losses can be expressed as

$$P_{\mathrm{Bd}}(\cdot) = s_{\mathrm{B}} n_0 R_c i_c^2(t) = R_c C_c \frac{P_{\mathrm{B}}^2(t)}{2E_{\mathrm{B}}(t) + s_{\mathrm{B}} n_0 C_c u_{c0}^2} \tag{10}$$

which, as quadratic-over-linear, is a convex function of $P_{\mathrm{B}}(t)$, $E_{\mathrm{B}}(t)$ and s_{B} [Boyd and Vandenberghe, 2004], for a strictly positive denominator.

Constraints on SOC and cell current translate to constraints on pack energy and power

$$E_{\mathrm{B}}(t) \in s_{\mathrm{B}} \frac{n_0 C_c}{2}\left(\left[u_c^2(\mathrm{soc}_{\min}), u_c^2(\mathrm{soc}_{\max})\right] - u_{c0}^2\right) \tag{11}$$

$$P_{\mathrm{B}}(t) \in [i_{\mathrm{cmin}}, i_{\mathrm{cmax}}]\sqrt{s_{\mathrm{B}} n_0 \left(\frac{2E_{\mathrm{B}}(t)}{C_c} + s_{\mathrm{B}} n_0 u_{c0}^2\right)} \tag{12}$$

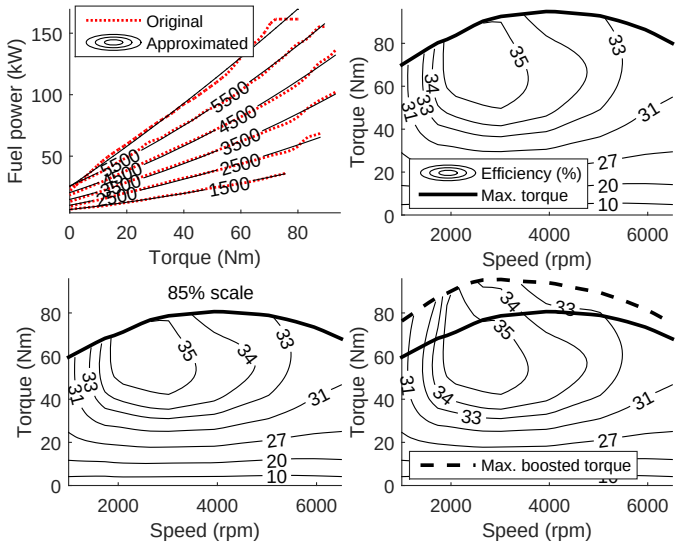

Fig. 3. Static model of a 4-stroke gasoline engine. Top left: original and approximated fuel power vs. torque, for different engine speeds in rpm. Top right: efficiency map of the approximated model. Bottom left: efficiency map of an 85 % scaled engine. Bottom right: efficiency map of a supercharged 85 % scaled engine.

where the geometric mean in (12) is a concave function of $E_{\mathrm{B}}(t)$ and s_{B} [Boyd and Vandenberghe, 2004]. The battery dynamics are simply expressed as

$$\dot{E}_{\mathrm{B}}(t) = -P_{\mathrm{B}}(t). \tag{13}$$

In the case when $u_{c0} = 0$ the model (10)-(13) would describe a capacitor. For a full derivation of this model see Murgovski et al. [2012b] and Egardt et al. [2014].

3.3 Electrically supercharged ICE

The model for the scaled and supercharged ICE is derived from the model of an existing, baseline ICE. As a baseline we use a 4-stroke naturally aspirated gasoline engine, whose net torque $\tau_{\mathrm{E0}}(t)$ is limited by

$$\tau_{\mathrm{E0}}(t) \in [0, \tau_{\mathrm{Emax0}}(\omega_{\mathrm{E}})]. \tag{14}$$

The fuel power of the baseline ICE is modeled by a static, second order function

$$P_{f0}(\cdot) = a_0(\omega_{\mathrm{E}}) + a_1(\omega_{\mathrm{E}})\tau_{\mathrm{E0}}(t) + a_2(\omega_{\mathrm{E}})\tau_{\mathrm{E0}}^2(t) \tag{15}$$

with coefficients parameterized in engine speed. Furthermore, $a_2(\omega_{\mathrm{E}}) \geq 0, \forall \omega_{\mathrm{E}}$, implying that the fuel power is a convex function of engine torque. This is a common way of modeling the ICE, known as Willans approximation [Guzzella and Onder, 2010]. Even a simpler representation, affine in torque, is often considered an accurate representation [Guzzella and Onder, 2010]. The fit of the fuel power approximation and the corresponding efficiency plot are depicted in the top left and top right plots of Fig. 3.

The ICE is downsized by scaling the displacement volume V_{d0} of the baseline ICE, while keeping the bore-to-stroke ratio constant. Since engine torque depends linearly on the displacement volume,

$$\tau_{\mathrm{Emax0}} = \frac{V_{d0}}{4\pi} p_{\mathrm{ime0}}(\omega_{\mathrm{E}}) \tag{16}$$

it follows that the torque of the scaled engine relates linearly to the torque of the baseline engine, $\tau_{\mathrm{E}}(t) = s_{\mathrm{E}}\tau_{\mathrm{E0}}(t)$, while maintaining the same operational speed range [Guzzella and Onder, 2010]. Here, $p_{\mathrm{ime0}}(\omega_{\mathrm{E}})$ is the indicated mean effective pressure. The fuel power is assumed to also scale linearly

$$\begin{aligned} P_f(\cdot) &= s_{\mathrm{E}} P_{f0}(\cdot) \\ &= a_0(\omega_{\mathrm{E}})s_{\mathrm{E}} + a_1(\omega_{\mathrm{E}})\tau_{\mathrm{E}}(t) + a_2(\omega_{\mathrm{E}})\frac{\tau_{\mathrm{E}}^2(t)}{s_{\mathrm{E}}} \end{aligned} \tag{17}$$

which means that the same efficiency map of the baseline ICE is used, but only stretched/compressed to the scaled torque limit. Similar modelling approximation has been used by Sundström [2009], Pourabdollah et al. [2013]. The efficiency map of a scaled engine is illustrated in the bottom left plot of Fig. 3.

Equation (17) can be recognized as a perspective function of (15). Thus, it is convex in both $\tau_{\mathrm{E}}(t)$ and s_{E} [Boyd and Vandenberghe, 2004].

In addition to scaling, the engine torque in (16) can be also increased by increasing the indicated mean effective pressure $p_{\mathrm{ime0}}(\omega_{\mathrm{E}})$. This can be achieved by using a compressor to boost the pressure at the engine inlet manifold. Considering ambient pressure and temperature, p_a, T_a, at the compressor inlet, and denoting with $\Pi(t) = p_{\mathrm{C}}(t)/p_a$ the pressure ratio over the compressor, with $p_{\mathrm{C}}(t)$ being the pressure at the compressor outlet, the compressor power can be expressed as

$$P_{\mathrm{C}}(\cdot) = \dot{m}_{\mathrm{C}}(t) c_p \frac{T_a}{\eta_{\mathrm{C}}} \left(\Pi(t)^{\frac{\kappa-1}{\kappa}} - 1\right) \tag{18}$$

with

$$\dot{m}_{\mathrm{C}}(t) = \eta_V \frac{V_d \omega_{\mathrm{E}}(t) p_{\mathrm{C}}(t)}{4\pi R_a T_{\mathrm{C}}(t)}, \tag{19}$$

while the temperature increase due to compression,

$$T_{\mathrm{C}}(t) = T_a + \frac{T_a}{\eta_{\mathrm{C}}} \left(\Pi(t)^{\frac{\kappa-1}{\kappa}} - 1\right) \tag{20}$$

where $\dot{m}_{\mathrm{C}}(t)$, c_p, κ and R_a are air mass flow, specific heat capacity, specific heat ratio and specific gas constant of air, respectively [Guzzella and Onder, 2010]. The air mass flow in (19) is derived by considering a stoichiometric air-fuel ratio. The isentropic compressor efficiency and the volumetric efficiency are denoted by η_{C} and η_V, respectively, and are assumed to be constant.

The ratio of torque increase due to supercharging, $s_{\Pi}(\cdot)$, is computed as the ratio of airmass flow (19) between the supercharged and naturally aspirated engine at wide open throttle [Banish, 2009]

$$s_{\Pi}(\cdot) = \frac{\eta_V \frac{V_d \omega_{\mathrm{E}}(t) p_{\mathrm{C}}(t)}{4\pi R_a T_{\mathrm{C}}(t)}}{\eta_V \frac{V_d \omega_{\mathrm{E}}(t) p_a}{4\pi R_a T_a}} = \Pi(t)\frac{T_a}{T_{\mathrm{C}}(t)}. \tag{21}$$

Equations (18)-(21) are combined to obtain

$$s_{\Pi}(\Pi) = \frac{\Pi(t)}{1 + \frac{1}{\eta_{\mathrm{C}}}\left(\Pi(t)^{\frac{\kappa-1}{\kappa}} - 1\right)} \tag{22}$$

$$P_{\mathrm{C}}(\Pi, s_{\mathrm{E}}) = \beta \omega_{\mathrm{E}}(t) s_{\mathrm{E}} \left(\Pi(t) - s_{\Pi}(\Pi)\right) \tag{23}$$

where the displacement volume of the downsized engine ($s_{\mathrm{E}} \leq 1$) is replaced with $V_d = s_{\mathrm{E}} V_{d0}$ and $\beta = \eta_V p_a c_p V_{d0}/(4\pi R_a)$. Finally, the torque limits of the scaled and supercharged ICE are expressed by

$$\tau_{\mathrm{E}}(t) \in [0, \tau_{\mathrm{Emax0}}(\omega_{\mathrm{E}}) s_{\mathrm{E}} s_{\Pi}(\Pi)]. \tag{24}$$

The fuel power relation (17) is assumed identical for both the naturally aspirated and the supercharged engine operation. This is a pessimistic model, since it has been indicated by Hiereth and Prenninger [2007], Martin et al. [2014] that the supercharged engine has a better effective efficiency than a naturally aspirated engine. The assumption will have little influence on the results, since only a small fraction of the driving cycle sampled points are operated under supercharged conditions, as it will be shown later, in Section 5.

The efficiency map of a supercharged engine is illustrated in the bottom right plot of Fig. 3.

3.4 Problem formulation

The optimization objective is formulated to minimize a cost function consisting of operational and components costs. The operational cost is simply the cost for consumed petroleum and the components cost constitutes the cost for ICE and electric buffer. The two costs are weighted into a single objective function, where the weighting coefficients w_f, w_{E}, w_{B} transform the costs for petroleum, ICE and electric buffer into currency/km. More information on how these coefficients are computed can be found in Pourabdollah et al. [2013].

The resulting optimization problem can be summarized as follows

$$\min \quad w_f \int_0^{t_f} P_f(\tau_{\mathrm{E}}, s_{\mathrm{E}})dt + w_{\mathrm{E}} s_{\mathrm{E}} + w_{\mathrm{B}} s_{\mathrm{B}} \tag{25a}$$

s.t. (11), (12),

$$\tau_{\mathrm{E}}(t) + \tau_{\mathrm{brk}}(t) = \frac{P_{\mathrm{A}}(t)}{\omega_{\mathrm{E}}(t)\eta_{\mathrm{A}}} + \tau_d(s_{\mathrm{E}}, s_{\mathrm{B}}) \tag{25b}$$

$$P_{\mathrm{B}}(t) + P_{\mathrm{A}}(t) = P_{\mathrm{Bd}}(\cdot) + \frac{P_{\mathrm{C}}(\Pi, s_{\mathrm{E}})}{\eta_{\mathrm{M}}} + P_{\mathrm{aux}} \tag{25c}$$

$$\dot{E}_{\mathrm{B}}(t) = -P_{\mathrm{B}}(t) \tag{25d}$$

$$E_{\mathrm{B}}(0) = E_{\mathrm{B}}(t_f) \tag{25e}$$

$$\tau_{\mathrm{E}}(t) \in [0, \tau_{\mathrm{Emax0}}(\omega_{\mathrm{E}}) s_{\mathrm{E}} s_{\Pi}(\Pi)] \tag{25f}$$

$$\Pi(t) \in [1, \Pi_{\max}] \tag{25g}$$

$$P_{\mathrm{C}}(\Pi) \leq P_{\mathrm{Cmax}} \tag{25h}$$

$$P_{\mathrm{A}}(t) \in [0, P_{\mathrm{Amax}}] \tag{25i}$$

$$s_{\mathrm{B}} \geq 0, \quad s_{\mathrm{E}} \in [0, 1], \quad \tau_{\mathrm{brk}} \leq 0 \tag{25j}$$

where the constraints are imposed $\forall t \in [0, t_f]$ and t_f is the time when the trip ends. The conservation of buffer energy is constrained by (25e) and limits are imposed on the pressure ratio, compressor power, alternator power, scaling coefficients and braking torque, by (25g)-(25j). There are six time dependent optimization variables, $\tau_{\mathrm{E}}(t), \tau_{\mathrm{brk}}(t), P_{\mathrm{A}}(t), P_{\mathrm{B}}(t), E_{\mathrm{B}}(t), \Pi(t)$, and two scalar variables, s_{E} and s_{B}.

4. CONVEX MODELING

In this section we revisit the optimization problem (25) and we show that the problem can be reformulated as a convex second order cone program (SOCP).

4.1 The supercharging ratio as a concave function

An important aspect for the problem convexity discussed later, in Section 4.3, is that the supercharging ratio $s_{\Pi}(\Pi)$

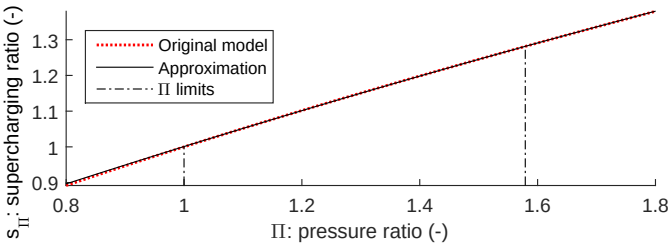

Fig. 4. Second order approximation of the supercharging ratio. The lines of the original and approximated model completely overlap.

is a concave function. By investigating the second derivative of $s_{\Pi}(\Pi)$,

$$\frac{d^2 s_{\Pi}(\Pi)}{d\Pi(t)^2} = \frac{\eta_{\mathrm{C}} \frac{\kappa-1}{\kappa} \Pi(t)^{\frac{-1}{\kappa}}}{(\eta_{\mathrm{C}} + \Pi(t)^{\frac{\kappa-1}{\kappa}} - 1)^2} \left(\frac{2\frac{\kappa-1}{\kappa} \Pi(t)^{\frac{\kappa-1}{\kappa}}}{\eta_{\mathrm{C}} + \Pi(t)^{\frac{\kappa-1}{\kappa}} - 1} - 2 + \frac{1}{\kappa} \right)$$

where the term left to the parenthesis is nonnegative, it can be concluded that the supercharging ratio is convex for

$$\Pi(t)^{\frac{\kappa-1}{\kappa}} / (1 - \eta_{\mathrm{C}}) \in [1, 2\kappa - 1] \tag{26}$$

and concave otherwise. However, since outlet compressor pressure is greater than ambient pressure, *i.e.,* $\Pi(t) \geq 1$, the function $s_{\Pi}(\Pi)$ is concave if the compressor efficiency satisfies

$$\eta_{\mathrm{C}} \geq 2(\kappa - 1)/(2\kappa - 1). \tag{27}$$

For a specific heat ratio $\kappa = 1.4$ and compressor efficiency of 60 % used in the case study in Section 5, the function $s_{\Pi}(\Pi)$ is concave in the entire feasible range of $\Pi(t)$, since $\eta_{\mathrm{C}} > 2(\kappa - 1)/(2\kappa - 1) = 44\,\%$.

In addition to obtaining a convex problem, this paper investigates a standard SOCP formulation. For this reason, the supercharging ratio is approximated by a second order concave function

$$\hat{s}_{\Pi}(\Pi) = b_0 + b_1 \Pi(t) + b_2 \Pi^2(t) \tag{28}$$

with $b_2 \leq 0$ and $b_0 = 1 - b_1 - b_2$. It can be observed in Fig. 4 that this function accurately approximates the supercharging ratio. In fact, for the depicted operating range of $\Pi(t)$, an affine approximation could also be satisfactory.

4.2 Change of variables

Further analysis of problem (25) reveals that the product $s_{\mathrm{E}} \hat{s}_{\Pi}(\Pi)$ that appears in (25f) is neither convex, nor concave function. A remedy to this matter is a variable change

$$\tilde{\Pi}(t) = s_{\mathrm{E}} \Pi(t) \tag{29}$$

that allows a scaling function to be defined

$$\tilde{s}_{\Pi}(\tilde{\Pi}, s_{\mathrm{E}}) = s_{\mathrm{E}} \hat{s}_{\Pi}(\Pi) = b_0 s_{\mathrm{E}} + b_1 \tilde{\Pi}(t) + b_2 \frac{\tilde{\Pi}^2(t)}{s_{\mathrm{E}}} \tag{30}$$

that combines the scaling of displacement volume and torque increase due to supercharging. The function $\tilde{s}_{\Pi}(\cdot)$ is a perspective function of (28) and it is, therefore, concave in both $\tilde{\Pi}(t)$ and s_{E}. The compressor power

$$P_{\mathrm{C}}(\tilde{\Pi}, s_{\mathrm{E}}) = \beta \omega_{\mathrm{E}}(t) \left(\tilde{\Pi}(t) - \tilde{s}_{\Pi}(\tilde{\Pi}, s_{\mathrm{E}}) \right) \tag{31}$$

is a convex function of $\tilde{\Pi}(t)$ and s_{E}.

4.3 Convex second order cone program

Finally, the problem (25) is reformulated as a convex optimization problem

$$\min \quad w_f \int_0^{t_f} P_f(\tau_{\mathrm{E}}, s_{\mathrm{E}})dt + w_{\mathrm{E}} s_{\mathrm{E}} + w_{\mathrm{B}} s_{\mathrm{B}} \tag{32a}$$

$$\text{s.t. } (11), (12), (25d), (25e), (25j), (25i)$$

$$\tau_{\mathrm{E}}(t) + \tau_{\mathrm{brk}}(t) = \frac{P_{\mathrm{A}}(t)}{\omega_{\mathrm{E}}(t)\eta_{\mathrm{A}}} + \tau_d(s_{\mathrm{E}}, s_{\mathrm{B}}) \tag{32b}$$

$$P_{\mathrm{B}}(t) + P_{\mathrm{A}}(t) \geq P_{\mathrm{Bd}}(\cdot) + \frac{P_{\mathrm{C}}(\tilde{\Pi}, s_{\mathrm{E}})}{\eta_{\mathrm{M}}} + P_{\mathrm{aux}} \tag{32c}$$

$$\tau_{\mathrm{E}}(t) \in [0, \tau_{\mathrm{Emax0}}(\omega_{\mathrm{E}})\tilde{s}_{\Pi}(\tilde{\Pi}, s_{\mathrm{E}})] \tag{32d}$$

$$\tilde{\Pi}(t) \in s_{\mathrm{E}}[1, \Pi_{\mathrm{max}}] \tag{32e}$$

$$P_{\mathrm{C}}(\tilde{\Pi}) \leq P_{\mathrm{Cmax}} \tag{32f}$$

where the electric power balance (25c) has been relaxed with inequality. The relaxation changes the original formulation, by creating a convex superset of the non-convex set. However, it can be logically reasoned that (32c) will hold with equality at the optimum, as otherwise energy will be wasted unnecessarily. Hence, the solution of the relaxed problem is also the solution of the non-relaxed problem. For a detailed proof see Murgovski et al. [2015].

The problem (32) is written in discrete time using zero order hold, and then it is casted to a standard SOCP form

$$\begin{aligned} &\text{minimize } f^T x \\ &\text{subject to } ||A_i x + e_i||_2 \leq c_i^T x + d_i, \qquad i = 1, .., .m \\ &\qquad\qquad Fx = g \end{aligned}$$

where $x \in R^n$ are optimization variables, $A_i \in R^{n_i \times n}$, $F \in R^{p \times n}$, and $||\cdot||_2$ is Euclidean norm. Constraints of type $z \geq x^2/y$ (or equivalently $\sqrt{yz} \geq x$) are written as

$$\left|\left| \begin{pmatrix} 2x \\ y - z \end{pmatrix} \right|\right|_2 \leq y + z. \tag{33}$$

Further details on SOCP modeling can be found in Boyd and Vandenberghe [2004]. The problem is solved with SeDuMi [Labit et al., 2002].

5. CASE STUDY

This section provides a case study of powertrain sizing on WLTP3. The ICE illustrated in the top right plot of Fig. 3 is used as a baseline. Two electric buffers are considered, a lithium-ion A123 battery cell and a Maxwell supercapacitor cell with specifications provided in Table 2. The costs for gasoline, battery and supercapacitor are 1.216 EUR/l, 500 EUR/kWh and 8000 EUR/kWh, respectively. Varying engine cost (that varies with size) is 0.67 EUR/kW. The remaining parameters are given in Table 3.

5.1 Gear selection strategy

Gear is decided outside the convex optimization, by an iterative search. First, gear is selected that maximizes the difference of engine operating points from the maximum torque line. This step allows the engine to be downsized as mush as possible, where engine and battery size is obtained by solving the convex problem (32) for the selected gear. Second, the obtained component sizes are used as a baseline for selecting gear that maximizes engine efficiency for the naturally aspirated operation. The convex problem (32) is solved to obtain new component sizes. These component sizes are used as a baseline in further iterations, where the second step is repeated until component sizes converge to a certain value. It was found that the optimal engine and buffer sizes converge in just two iterations.

More sophisticated gear selection strategies that also employ iterative solutions of convex problems have been published and could be applied to this problem as well [Pourabdollah et al., 2014, Nüesch et al., 2014].

Table 2. Electric buffer cell specifications.

Battery	Supercapacitor
$m_{\mathrm{Bc}} = 80\,\mathrm{g}$	$m_{\mathrm{Bc}} = 414\,\mathrm{g}$
$Q_c = 2.3\,\mathrm{Ah}$	$C_c = 2\,\mathrm{kF}$
$R_c = 11.5\,\mathrm{m\Omega}$	$R_c = 0.4\,\mathrm{m\Omega}$
$i_{\mathrm{cmin/max}} = \mp 35\,\mathrm{A}$	$i_{\mathrm{cmin/max}} = \mp 1600\,\mathrm{A}$
$\mathrm{soc}_{\mathrm{min/max}} = \{20, 80\}\,\%$	$\mathrm{soc}_{\mathrm{min/max}} = \{10, 100\}\,\%$
$w_{\mathrm{B}} = 0.0453\,\mathrm{EURc/km}$	$w_{\mathrm{B}} = 0.0062\,\mathrm{EURc/km}$
$C_c = 58\,\mathrm{kF}, u_{c0} = 3.27\,\mathrm{V}$	

Table 3. Vehicle specifications.

$A_f = 2.07\,\mathrm{m}^2$	$\rho_a = 1.184\,\mathrm{kg/m}^3$	$\eta_V = 90\,\%$
$c_d = 0.32$	$p_a = 101\,325\,\mathrm{Pa}$	$\eta_{\mathrm{C}} = 60\,\%$
$c_r = 0.01$	$\kappa = 1.4$	$\eta_{\mathrm{M}} = 92\,\%$
$\lambda = 1.3$	$c_p = 1005\,\mathrm{J/kgK}$	$\eta_\gamma = 95\,\%$
$P_{\mathrm{aux}} = 0\,\mathrm{W}$	$R_a = 287\,\mathrm{J/kgK}$	$\eta_{\mathrm{A}} = 65\,\%$
$m_0 = 970\,\mathrm{kg}$	$r_\gamma = \{15.2, 8.2, 5.3, 4, 3.3\}$	$P_{\mathrm{Amax}} = 1\,\mathrm{kW}$
$r_w = 29.57\,\mathrm{cm}$	$g = 9.81\,\mathrm{m/s}^2$	$\Pi_{\mathrm{max}} = 1.58$
$m_{\mathrm{E}} = 62.67\,\mathrm{kg}$	$w_{\mathrm{E}} = 0.019\,\mathrm{EURc/km}$	$b_1 = 0.61$
$V_{d0} = 1000\,\mathrm{cm}^3$	$w_f = 0.584\,\mathrm{EURc/kWh/km}$	$b_2 = -0.049$

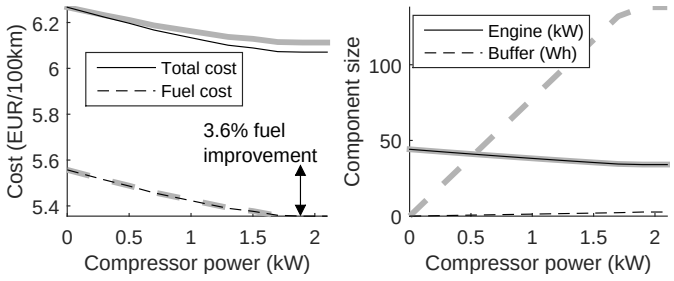

Fig. 5. Total and fuel cost, to the left, and component sizes, to the right. The thick lines depict results when using a battery, and thin lines when using a supercapacitor.

5.2 Optimal component sizes

The powertrain sizing problem is solved for different compressor powers ranging within $[0, 2]$ kW, where 0 corresponds to naturally aspirated operation. The results are shown in Fig. 5 for the two cases of using either the lithium-ion battery, or the supercapacitor. It is apparent that the supercharging decreases the fuel cost by about 3.6 %, for any of the two buffers, in spite of the pessimistic fuel model (17).

The total optimization cost for the two buffers, depicted in the left plot of Fig. 5, shows that the used battery technology is not the best choice, despite the much smaller cost per energy content. The right plot in Fig. 5 reveals that the operational (fuel) cost and engine sizes are nearly

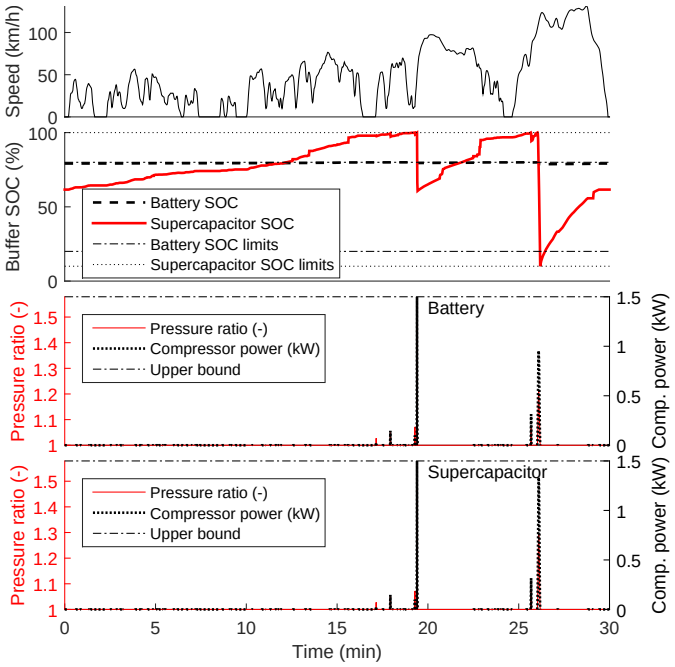

Fig. 6. From top to bottom: speed profile of the driving cycle, optimal buffer SOC trajectories, pressure ratio and compressor power when using a battery, and pressure ratio and compressor power when using a supercapacitor. The upper bound in the last two plots depicts both the pressure ratio limit and the compressor power limit.

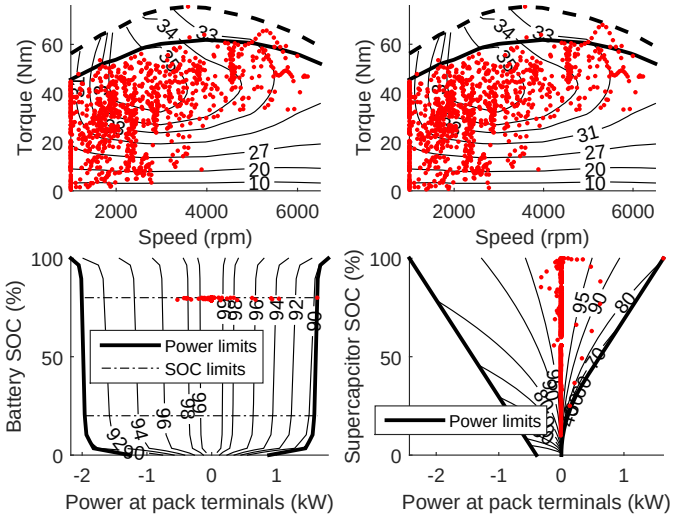

Fig. 7. Optimal operating points depicted by a dot marker. The top plot shows operating points for the ICE, and the bottom plot for the electric buffer. The left plots show results when using a battery, and the right when using a supercapacitor. The contour lines depict the efficiencies of the components.

identical for the two buffers, implying that the main difference in total cost is the buffer investment cost.

5.3 Optimal state and control trajectories

Apart from the optimal component sizes, the solution of problem (32) provides also the optimal control and state trajectories for the studied driving cycle. These are shown in Fig. 6 for the case when MCU power is 1.5 kW. Indeed, it can be observed that the compressor is operated at peak power for the operating point with the highest power demanded by the driving cycle. Although the MCU is operated similarly for the battery and supercapacitor scenario, there is a major difference in the state trajectories of these two buffers. Very little of the battery energy content is utilized and the battery SOC trajectory stays close to its upper limit, for which the open circuit voltage is higher and losses are thus lower. The battery is sized by the power requirements, which is visible in Fig. 7. This indicates that the chosen battery cell is not a good candidate for the studied application, and additional investigations should be performed for batteries with higher power to energy ratio. On the contrary, the supercapacitor is utilized in its entire power/energy operating range, as shown in Fig. 7.

6. DISCUSSION AND CONCLUSIONS

This paper provides convex modeling steps for the problem of optimally sizing the ICE and electric buffer (battery, or supercapacitor), while delivering high power demands by supercharging. The optimal solution provides also the optimal control and state trajectories that minimize operational cost on a given driving cycle. In the provided case study the driving cycle used to evaluate the engine concept is WLTP3, although the proposed method is the same for any other driving cycle. Ideally, the engine concept should be evaluated on a larger set of driving cycles that may better represent the typical usage of the target vehicle. These cycles could be appended into one long driving cycle, which may also include performance requirements, represented by, *e.g.,* acceleration vs. speed profiles, or additional constraints in the problem [Pourabdollah et al., 2013].

The powertrain model considers constant efficiencies for the alternator and the MCU, although problem convexity will be preserved if their losses are modeled as any other function convex in power/torque. Including thermal states for the ICE and MCU without infringing convexity is also possible [Murgovski et al., 2012a], and will be the subject of future studies. Future studies may also include investigations of other electric buffer cell technologies, including constraints on the pack terminal voltage.

REFERENCES

D. Assanis, G. Delagrammatikas, R. Fellini, Z. Filipi, J. Liedtke, N. Michelena, P. Papalambros, D. Reyes, D. Rosenbaum, A. Sales, and M. Sasena. An optimization approach to hybrid electric propulsion system design. *Journal of Mechanics of Structures and Machines, Automotive Research Center Special Edition*, 27(4):393–421, 1999.

G. Banish. *Designing and Tuning High-Performance Fuel Injection Systems*. CarTech, 2009.

S. Boyd and L. Vandenberghe. *Convex Optimization*. Cambridge University Press, 2004.

N. Chayopitak, R. Pupadubsin, S. Karukanan, and P. Champa. Design of a 1.5 kW high speed switched reluctance motor for electric supercharger with optimal performance assessment. In *15th International Confer-*

ence on Electrical Machines and Systems, pages 1–5, Sapporo, 2012.

B. Egardt, N. Murgovski, M. Pourabdollah, and L. Johannesson. Electromobility studies based on convex optimization: Design and control issues regarding vehicle electrification. *IEEE Control Systems Magazine*, 34(2): 32–49, 2014.

H. Fathy, P. Papalambros, and A. Ulsoy. On combined plant and control optimization. In *8th Cairo University International Conference on Mechanical Design and Production*, Cairo University, 2004.

Z. Filipi, L. Louca, B. Daran, C.-C. Lin, U. Yildir, B. Wu, M. Kokkolaras, D. Assanis, H. Peng, P. Papalambros, J. Stein, D. Szkubiel, and R. Chapp. Combined optimisation of design and power management of the hydraulic hybrid propulsion systems for the 6 x 6 medium truck. *International Journal of Heavy Vehicle Systems*, 11(3): 372–402, 2004.

N. Fraser, H. Blaxill, G. Lumsden, and M. Bassett. Challenges for increased efficiency through gasoline engine downsizing. *SAE Int. J. Engines*, 2:991–1008, 2009.

V. Galdi, L. Ippolito, A. Piccolo, and A. Vaccaro. A genetic-based methodology for hybrid electric vehicles sizing. *Soft Computing - A Fusion of Foundations, Methodologies and Applications*, 5(6):451–457, 2001.

L. Guzzella and C. H. Onder. *Introduction to Modeling and Control of Internal Combustion Engine Systems*. Springer-Verlag, 2010.

L. Guzzella and A. Sciarretta. *Vehicle Propulsion Systems*. Springer, Verlag, Berlin, Heidelberg, 3 edition, 2013.

H. Hiereth and P. Prenninger. *Charging the Internal Combustion Engine*. Springer, 2007.

S. Kachapornkul, P. Somsiri, R. Pupadubsin, and N. Nulek. Low cost high speed switched reluctance motor drive for supercharger applications. In *15th International Conference on Electrical Machines and Systems*, pages 1–6, Sapporo, 2012.

M. Kim and H. Peng. Power management and design optimization of fuel cell/battery hybrid vehicles. *Journal of Power Sources*, 165(2):819–832, 2007.

Y. Labit, D. Peaucelle, and D. Henrion. SeDuMi interface 1.02: a tool for solving LMI problems with SeDuMi. *IEEE International Symposium on Computer Aided Control System Design Proceedings*, pages 272–277, 2002.

P. Leduc, B. Dubar, A. Ranini, and G. Monnier. Downsizing of gasoline engine: an efficient way to reduce CO2 emissions. *Oil & Gas Science and Technology*, 58(1): 115–127, 2003.

S. Martin, C. Beidl, and R. Mueller. Responsiveness of a 30 bar BMEP 3-cylinder engine: Opportunities and limits of turbocharged downsizing. Technical Paper 2014-01-1646, SAE International, 2014.

N. Murgovski, L. Johannesson, A. Grauers, and J. Sjöberg. Dimensioning and control of a thermally constrained double buffer plug-in HEV powertrain. In *51st IEEE Conference on Decision and Control*, Maui, Hawaii, 2012a.

N. Murgovski, L. Johannesson, and J. Sjöberg. Convex modeling of energy buffers in power control applications. In *IFAC Workshop on Engine and Powertrain Control, Simulation and Modeling (E-CoSM)*, Rueil-Malmaison, Paris, France, 2012b.

N. Murgovski, L. Johannesson, J. Sjöberg, and B. Egardt. Component sizing of a plug-in hybrid electric powertrain via convex optimization. *Mechatronics*, 22(1):106–120, 2012c.

N. Murgovski, L. Johannesson, X. Hu, B. Egardt, and J. Sjöberg. Convex relaxations in the optimal control of electrified vehicles. In *American Control Conference*, Chicago, USA, 2015.

T. Nüesch, P. Elbert, M. Flankl, C. Onder, and L. Guzzella. Convex optimization for the energy management of hybrid electric vehicles considering engine start and gearshift costs. *Energies*, 7(2):834–856, 2014.

D. L. Peters, P. Y. Papalambros, and A. G. Ulsoy. Sequential co-design of an artifact and its controller via control proxy functions. *Mechatronics*, 23(4):409–418, 2013.

M. Pourabdollah, N. Murgovski, A. Grauers, and B. Egardt. Optimal sizing of a parallel PHEV powertrain. *IEEE Transactions on Vehicular Technology*, 62 (6):2469–2480, 2013.

M. Pourabdollah, N. Murgovski, A. Grauers, and B. Egardt. An iterative dynamic programming/convex optimization procedure for optimal sizing and energy management of PHEVs. In *IFAC World Congress*, pages 6606–6611, Cape Town, South Africa, 2014.

J. A. Reyer and P. Y. Papalambros. Combined optimal design and control with application to an electric DC motor. *Journal of Mechanical Design*, 142(2):183–191, 2002.

S. Shahed and K. Bauer. Parametric studies of the impact of turbocharging on gasoline engine downsizing. In *SAE World Congress & Exhibition*, volume 2, pages 1347–1358. SAE International, 2009.

O. Sundström. *Optimal control and design of hybrid-electric vehicles*. PhD thesis, Institute for Dynamic Systems and Control, ETH Zurich, 2009.

O. Sundström, L. Guzzella, and P. Soltic. Torque-assist hybrid electric powertrain sizing: From optimal control towards a sizing law. *IEEE Transactions on Control Systems Technology*, 18(4):837–849, 2010.

E. Tara, S. Shahidinejad, S. Filizadeh, and E. Bibeau. Battery storage sizing in a retrofitted plug-in hybrid electric vehicle. *IEEE Transactions on Vehicular Technology*, 59 (6):2786–2794, 2010.

B. Taylor and D. Howe. Experimental characterization of a supercapacitor-based electrical torque-boost system for downsized ICE vehicles. *IEEE Transactions on Vehicular Technology*, 56(6):3674–3681, 2007.

J. Villegas, B. Gao, K. Svancara, W. Thornton, and J. Parra. Real-time simulation and control of an electric supercharger for engine downsizing. In *IEEE Vehicle Power and Propulsion Conference*, pages 1–6, 2011.

J. Wang, Z. Xia, and D. Howe. Three-phase modular permanent magnet brushless machine for torque boosting on a downsized ICE vehicle. *IEEE Transactions on Vehicular Technology*, 54(3):809–816, 2005.

L. Wu, Y. Wang, X. Yuan, and Z. Chen. Multiobjective optimization of HEV fuel economy and emissions using the self-adaptive differential evolution algorithm. *IEEE Transactions on Vehicular Technology*, 60(6):2458–2470, 2011.